Spin-wave emission and propagation in a magnetically nanopatterned thick Synthetic Antiferromagnet

Davide Girardi[1]*, Simone Finizio[2], Claire Donnelly[3], Guglielmo Rubini[1], Sina Mayr[2,4], Valerio Levati[1], Simone Cuccurullo[1], Federico Maspero[5,6], Jörg Raabe[2], Daniela Petti[1]*, Edoardo Albisetti[1]*

[1]Dipartimento di Fisica, Politecnico di Milano; Piazza Leonardo da Vinci 32, Milano 20133, Italy.

[2]Swiss Light Source, Paul Scherrer Institut; Forschungsstrasse 111 5232 PSI Villigen, Switzerland.

[3]Max Planck Institute for Chemical Physics of Solids; Nöthnitzer Str. 40, 01187 Dresden, Germany.

[4]Laboratory for Mesoscopic Systems, Department of Materials, ETH Zurich, 8093 Zurich, Switzerland.

[5]Dipartimento di Ingegneria Civile e Ambientale, Politecnico di Milano; Piazza Leonardo da Vinci 32, Milano 20133, Italy.

[6]Istituto di Fotonica e Nanotecnologie, Consiglio Nazionale delle Ricerche (CNR-INF); Piazza Leonardo da Vinci 32, Milano 20133, Italy.

*Corresponding author. Email: davide.girardi@polimi.it (DG); daniela.petti@polimi.it (DP); edoardo.albisetti@polimi.it (EA)

ABSTRACT

Spin-wave based devices offer several advantages, such as the absence of Joule losses and the sub-μm wavelength in the GHz-THz range, and have been proposed as promising alternatives to the standard CMOS technology. In this context, synthetic antiferromagnetic systems have been extensively studied for the development of nanomagnonic devices, thanks to their high degree of tunability. Moreover, spin textures have recently been demonstrated as efficient means for the generation and emission of spin waves. Here, we show that with the newly proposed phase nanoengineering methodology it is possible to magnetically nanopattern spin textures via thermally assisted magnetic Scanning Probe Lithography in a 200 nm thick exchange-biased synthetic antiferromagnetic multilayer. In such nanopatterned structures, we demonstrate via time-resolved Scanning Transmission X-Ray Microscopy the generation and manipulation of different types of coherent spin-wave modes. By strongly enhancing the robustness and quality of the spin-wave wavefronts propagating for multiple wavelengths in thick synthetic antiferromagnetic systems, this work opens the possibility to expand the comprehension of the spin-wave phenomenology also to the third dimension and to study the complex spin-wave properties through the volume of the magnetic systems, enabling their control for the design of novel three-dimensional nanomagnonic devices.

Keywords: Magnonics, spin waves, synthetic antiferromagnets, phase nanoengineering, Scanning Probe Lithography, spin textures, Scanning Transmission X-Ray Microscopy (STXM).

1. INTRODUCTION

Spin waves, also known as magnons, are dynamic wave-like perturbations of the magnetic texture, and have been extensively studied in the last decade in various systems as efficient alternatives to conventional electronics[1–3]. Due to the absence of Joule losses, and their sub-μm wavelength in the GHz-THz frequency range, magnons have been proposed for

Spintronics XVI, edited by Jean-Eric Wegrowe, Joseph S. Friedman, Manijeh Razeghi, Proc. of SPIE Vol. 12656, 126560F
© 2023 SPIE · 0277-786X · doi: 10.1117/12.2672913

the development of information carrier devices, for both analog and digital computation and signal processing, as well as for unconventional computational frameworks, such as neuromorphic and reservoir computing[3–11]. In this context, synthetic antiferromagnets (SAFs)[12,13], i.e. magnetic structures characterized by two ferromagnetic layers antiparallelly coupled at remanence via interlayer exchange coupling due to the presence of a non-magnetic interlayer, are promising systems for the development of different types of magnonic devices, thanks to their very high degree of tunability[14–16]. In addition to this, the non-reciprocity of spin waves in SAFs, arising from the dipolar coupling between the two ferromagnetic layers, allows to have high-quality spin-wave wavefronts due to the absence of back-reflections from physical boundaries[17,18]. Furthermore, the possibility to emit spin waves that propagate for multiple wavelengths from spin textures[19] such as vortices or domain walls has recently been demonstrated, and is extremely promising for the development of efficient nanomagnonic devices[18,20,21]. However, while a lot of research has been focused on studying the propagation of spin waves in thin synthetic antiferromagnetic structures, up to few tens of nanometers thick, a clear picture of their behavior for systems with thickness up to hundreds of nm is still missing[22].

In this work, we first use the newly developed methodology called phase nanoengineering[23] to magnetically nanopattern spin textures via thermally assisted magnetic Scanning Probe Lithography (tam-SPL)[18–21,24], in order to efficiently generate and manipulate spin-wave wavefronts, and then we study their emission and propagation in an exchange-biased synthetic antiferromagnetic multilayer 200 nm thick via time-resolved Scanning Transmission X-Ray Microscopy (STXM).

2. SAMPLE FABRICATION AND CHARACTERIZATION

The exchange-biased[25–27] synthetic antiferromagnetic structure is shown in Fig. 1a and consists of a $Co_{40}Fe_{40}B_{20}(100)$ / Ru(0.5) / $Co_{40}Fe_{40}B_{20}(100)$ / $Ir_{22}Mn_{78}(10)$ / Ru(2) (thickness in nm) stack grown by magnetron sputtering (AJA ATC Orion 8 system) in RF and DC mode with pressure below 1×10^{-8} Torr[15,16,18]. The sample was deposited on top of X-Ray transparent Si_3N_4 membrane 200 nm thick with variable size between 0.5×0.5 mm^2 and 1.0×1.0 mm^2, in order to allow the experiments in transmission. The Si_3N_4 membranes were previously nanopatterned with nine 100×100 μm^2 squared nanostructures by electron-beam lithography using a 100kV Vistec EBPG 5000Plus, as shown in Fig. 1c. In order to set the direction of the magnetocrystalline anisotropy and of the exchange bias, an in-plane magnetic field was applied during the deposition process. In addition to this, the sample underwent a field cooling procedure in a chamber with pressure below 10^{-4} mbar at 250°C for 5 minutes, in an in-plane magnetic field of 4 kOe oriented in the same direction as the one applied during the deposition. The normalized hysteresis loop along the easy axis was measured via a vibrating sample magnetometer (Microsense, LLC. Easy VSM) and is reported in Fig. 1b. The green and light-blue arrows represent the direction of the magnetization **M** for the bottom and top ferromagnetic layers, respectively. For strong external positive (negative) field, the magnetization of the ferromagnetic layers is parallelly coupled and saturated along the positive (negative) direction. Decreasing the field, the RKKY-mediated interlayer exchange coupling[28–30] forces the magnetization to align antiparallelly. This behavior is shown by the plateau at low fields. The sample displays a sizeable interlayer exchange coupling field $\mathbf{H_{ex}}$ of 105 Oe and a saturation field $\mathbf{H_{sat}}$ of 230 Oe. Specifically, the value of the saturation field $\mathbf{H_{sat}}$ is identified for **M** equal to 0.9 a.u. in the graph, while the interlayer exchange coupling field $\mathbf{H_{ex}}$ is calculated as the point between the plateau and $\mathbf{H_{sat}}$.

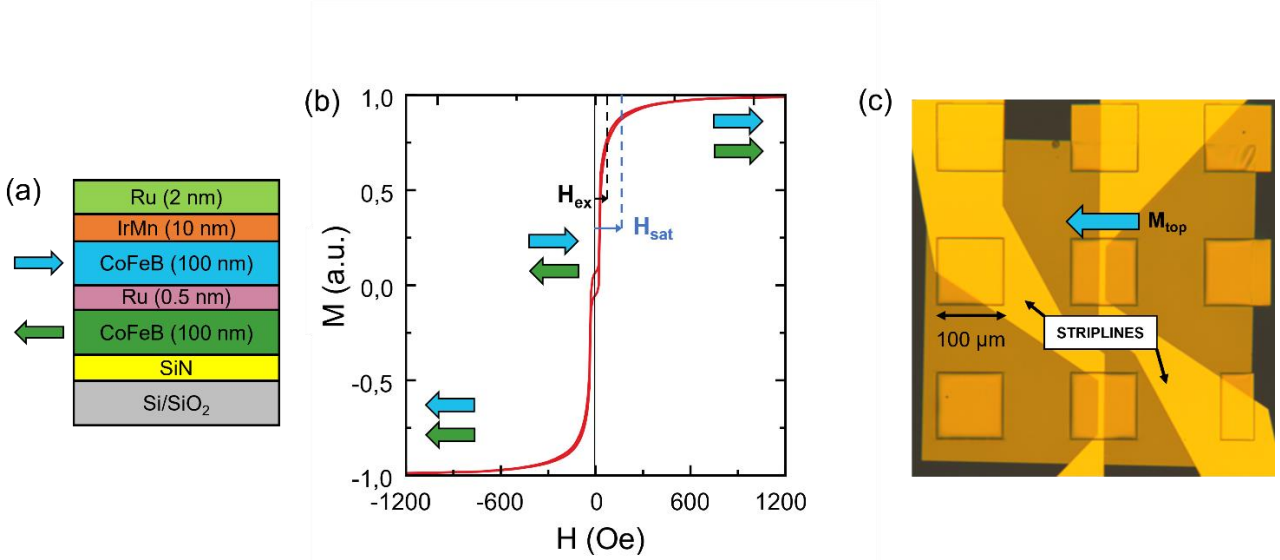

Figure 1: a. Sketch of the IrMn/CoFeB/Ru/CoFeB based exchange-biased synthetic antiferromagnetic (SAF) structure. The light-blue and green arrows depict the antiparallel coupling of the magnetization of the two ferromagnetic layers at remanence. b. Normalized hysteresis loop of the structure measured along the easy axis after field cooling, measured via Vibrating Sample Magnetometry. The light-blue and green arrows show the direction of the magnetization of the two ferromagnetic layers. c. Optical image of the Si_3N_4 membrane, of the 100 × 100 µm^2 nanopatterned squared structures with the SAF system deposited on top and of the Cu stripline for the excitation of the spin waves. The blue arrow shows the orientation of the in-plane magnetization of the top CoFeB layer.

In order to excite spin waves, on top of the SAF sample a 5 µm wide and 300 nm thick Cu stripline was patterned by electron beam lithography followed by lift-off using a Vistec EBPG5000 100 kV electron beam writer, as indicated in Fig. 1c. A bilayer resist composed of a layer of methyl methacrylate (6% dilution in ethyl-lactate, spincoated at 3000 rpm for one minute) followed by a layer of poly(methyl metachrylate) (4% dilution in Anisole, spincoated at 3000 rpm for one minute) was spincoated on top of the membrane. Following the spin coating, a soft bake at 175 °C for one minute was performed. The samples were finally exposed with a dose of 1500 µC/cm^2 and developed for 45 s by immersion in a 1:3 volume solution of methyl-isobutyl-ketone and isopropyl alcohol, followed by a 90 s immersion in pure isopropyl alcohol. The Cu film was deposited by thermal evaporation using a Balzers BAE250 evaporator.

3. MAGNETIC NANOPATTERNING VIA tam-SPL

In order to successfully excite and control spin waves in the system, domain walls were magnetically nanopatterned with the phase nanoengineering methodology via tam-SPL[18,20,21,23,24]. The tam-SPL working principle consists in locally altering the exchange bias field established between the adjacent antiferromagnetic and ferromagnetic layers, by sweeping the hot tip of a scanning probe microscope in contact with the sample, while an externally applied magnetic field is present, as depicted in Fig. 2a-c. Specifically, to shift the exchange bias, a local field cooling procedure is performed: the temperature of the tip is increased above the blocking temperature T_B of the structure, while an external applied magnetic field is present, as shown in Fig. 2b. This leads to the switching of the magnetization in the ferromagnetic layers. As the tip is displaced, the heated region slowly cools down, the exchange bias of the ferromagnetic layer in contact with the antiferromagnet is locally reset alongside the direction of the external field in the patterned region, and the interlayer exchange coupling forces the magnetization of the two ferromagnetic layers back in the antiparallel configuration (Fig. 2c). The procedure was performed using a customized Keysight 5600LS scanning probe system, equipped with silicon cantilevers integrated with a Joule-heating resistive heater. A National Instruments DAQ NI USB-6211 in combination with MATLAB scripts and Keysight PicoView software were employed for controlling the heater temperature and the tip movement. To pattern the magnetic domains, the tip was swept above the surface in a raster-scan fashion. A range of voltages was applied in different positions of the patterned membranes, aiming at creating domains with different

dimensions, ranging from 10 μm to 40 μm. An example of one of the resulting patterned domains in one of the 100 × 100 μm^2 squared nanostructures is reported in Fig. 2d, were an image taken with a Magneto-Optic Kerr Effect Microscope (μ-MOKE) is shown. The black-and-white contrast represents the different orientations of the in-plane component of the magnetization for the top CoFeB layer, which are further highlighted by the blue and red arrows, showing the direction of the magnetization of the top ferromagnetic layer after the deposition and of the magnetically nanopatterned domain, respectively. Finally, the domain walls used to control the emission of spin waves in the SAF are underlined by the white dotted line. Importantly, the possibility to stabilize magnetic domains in such thick synthetic antiferromagnetic systems is a consequence not only of the exchange bias interaction between the antiferromagnetic IrMn layer and the top ferromagnetic CoFeB layer, which is small in this thick structure since it is an interfacial interaction, but also of the antiferromagnetic coupling between the two layers, that allows to reduce the magnetostatic energy via the flux-closure state established inside the SAF structure itself.

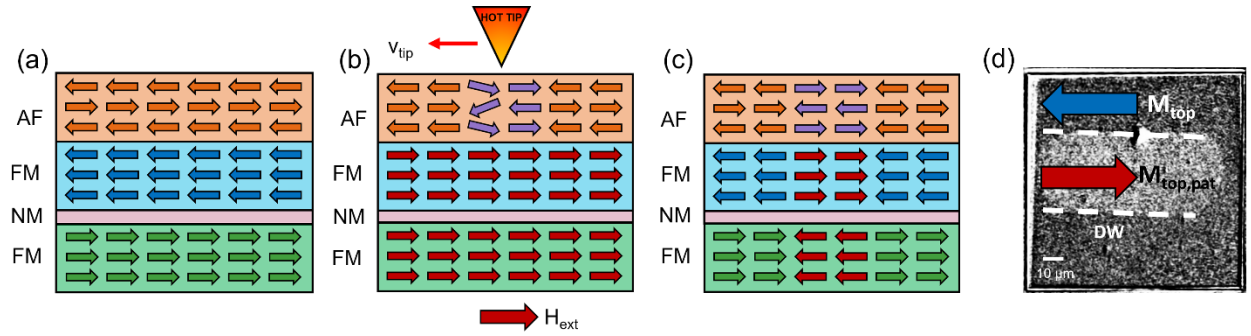

Figure 2: Magnetic nanopatterning of the exchange-biased synthetic antiferromagnetic (SAF) system using the phase nanoengineering methodology via thermally assisted magnetic Scanning Probe Lithography. a. After the deposition process, the magnetization of the two ferromagnetic layers is antiparallelly coupled (blue and green arrows) and the exchange bias interaction is established between the antiferromagnetic layer and the top ferromagnetic one. b. Sweeping the hot tip of a Scanning Probe Microscope on the sample surface in presence of an external magnetic field H_{ex}, a local field cooling procedure is performed which resets the exchange bias direction aligning the direction of the magnetization of the ferromagnetic layers with H_{ex} (red arrows). c. By removing the tip and the external field, the nanopatterned magnetic configuration of the SAF is stabilized (red arrows) by the exchange bias and by the flux closure state established inside the structure. d. μ-MOKE image of a magnetically nanopatterned domain at remanence. The blue and red arrow show the direction of the magnetization after the deposition and of the locally patterned domain for the top CoFeB layer, respectively.

4. EMISSION AND PROPAGATION OF SPIN WAVES IN MAGNETICALLY NANOPATTERNED SPIN TEXTURES

The spin waves emission and propagation from the magnetically nanopatterned spin textures was measured via time-resolved Scanning Transmission X-Ray Microscopy (STXM) at the PolLux (X07DA) endstation of the Swiss Light Source, at the Paul Scherrer Institut (PSI). To obtain the images, monochromatic X-Rays were tuned at the Co L_3 absorption edge (with photon energy of about 781 eV) and focused using an Au Fresnel zone plate onto a spot on the sample. The transmitted photons were recorded through an avalanche photodiode positioned behind the sample, which was raster-scanned using a piezoelectric stage. In order to obtain magnetic contrast, the X-Ray Magnetic Circular Dichroism (XMCD) effect was exploited, illuminating the sample with circularly polarized light. To probe the out-of-plane component of the magnetization, the sample was mounted such that the incoming X-Ray beam was perpendicular to the surface of the sample. For the time-resolved images, a pump-probe method was employed, in which the RF magnetic field, generated injecting a RF current in the patterned striplines corresponded to the pump signal, while the X-Rays generated by the synchrotron light to the probe one. For the time-resolved measurement, the pumping signal was synchronized by a field programmable gate array (FPGA) to the master clock of the synchrotron light source at 0.5 GHz. The accessible frequencies, due to the specific requirements of the FPGA available, correspond to f_{ex} = 0.5 × M/N GHz, where N is a prime number in this case selected equal to 7 (meaning each video is composed of 7 frames), and M is a positive integer. The resulting phase resolution was equal to 50°, while the temporal resolution, depending on the value of M, is equal to

2/M ns, with a lower limit of 70 ps FWHM, depending on the width of the X-Ray pulse generated by the synchrotron light source.

In the synthetic antiferromagnetic system developed, the interlayer exchange coupling and the dipolar interaction lead to the formation of coupled coherently propagating acoustic spin-wave modes in the two layers, characterized by antiparallel in-plane and parallel out-of-plane components of the magnetization, as sketched in Fig. 3b. For this reason, the in-phase oscillation for the z-component sums up between the two layers, thus allowing its measurement, while the out-of-phase oscillation for the x- and y-components gives a total magnetization equal to zero in the x-y plane. Figure 3a displays the resulting STXM image of emitted and propagating spin waves at 0.5 GHz with a spatial resolution of 50 nm. The domain wall is visible and the tilting of the magnetization in opposite out-of-plane directions on the two sides of the domain wall is given by the black-and-white contrast; the orientation of the in-plane magnetization is further highlighted in the image by the black arrows. Similarly, the contrast corresponds to the oscillations of the out-of-plane component of the magnetization and is associated with the propagation of spin waves in the sample. In addition to this, it is possible to clearly recognize the presence of a magnetic vortex on the right from the change in magnetic contrast in the domain wall. Both the domain wall and the vortex act as spin-wave emitters in this region, and are indicated in red (number 1) and light blue (number 2), respectively. Noticeably, the borders of the stripline itself that are crossing the patterned region, indicated in yellow (number 3), act as additional spin-wave emitters. Multiple propagation modes are generated from these emitters, and have been highlighted in the figure. Planar 2D spin-wave wavefronts are emitted from the domain wall (in red, letter A in figure). Remarkably, it is possible to observe that the wavefronts precisely follow the shape of the domain wall, which is slightly curving in this region. Furthermore, planar 2D wavefronts are emitted also from the borders of the stripline (in yellow, letter B) and are propagating in the region. The direction of propagation of these wavefronts is perpendicular to the direction of propagation of the spin waves emitted from the domain wall: this leads to the creation of a spin-wave interference region, underlined by the white dashed rectangle in figure (letter C). On the other hand, the vortex emits radial wavefronts, which are shown in the figure by the light blue dashed rectangle (letter D). Finally, it is interesting to note that spin waves are not only propagating in the magnetic domain, but are also confined inside the domain wall itself, as shown in green (letter E). These spin waves, in contrast with the 2D planar ones propagating in the magnetic domain, can be effectively described as 1D spin waves. It is possible to plot the spatial profiles of the waves emitted from the domain wall and confined inside the domain wall itself, as reported in Fig.3c-d, respectively. Consistently to what has been found by Sluka et al.[16], the two spin-wave modes are characterized by a different wavelength at the same excitation frequency: while the 2D planar spin waves emitted by the domain wall and propagating inside the magnetic domain have a spin-wave wavelength of ~ 410 nm (Fig.3c), the 1D spin waves confined inside the domain wall have a slightly smaller wavelength, equal to ~350 nm (Fig.3d).

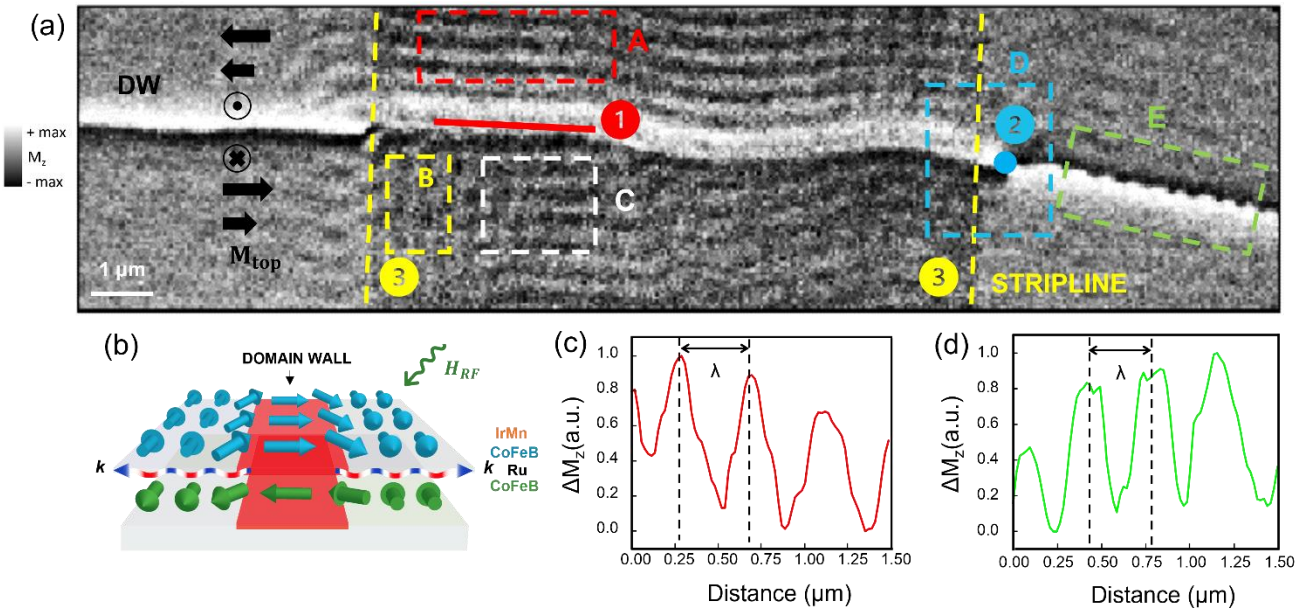

Figure 3: a. Scanning Transmission X-Ray Microscopy (STXM) image of emitted and propagating spin waves excited at 500 MHz with spatial resolution of 50 nm. The black-and-white contrast is used to represent the orientation of the out-of-plane component of the magnetization. The black arrows show the direction of **M** for the top CoFeB layer. The numbers and letters indicate different types of spin-wave emitters and modes, respectively. b. Sketch of spin waves in a synthetic antiferromagnet emitted from the domain wall and propagating in the magnetic domains. The spin-wave modes are excited by an external oscillating magnetic field (H_{RF}); the light-blue and green arrow show the orientation of the magnetization for the top and bottom CoFeB layers, respectively. c, d. Normalized spatial profiles of 2D planar spin waves emitted from the domain wall and propagating in the magnetic domain and 1D spin waves confined in the domain wall itself, respectively.

Figure 4a reports single time-resolved STXM frames of a zoomed region in which propagating spin waves are emitted from a domain wall at different frequencies, set equal to 0.43 GHz, 0.64 GHz, and 0.79 GHz, respectively. The domain wall is indicated in white, while the red and blue dotted lines show subsequent spin-wave wavefronts. In Fig. 4b the spatial profiles extracted from the green arrow indicating the spin-wave wavefronts are reported, from which it is possible to calculate the corresponding wavelengths, equal to 600 nm, 360 nm, and 300 nm for the three different frequencies, respectively. The results of the analysis on the behavior of propagating spin waves at different excitation frequencies is summarized in Fig. 4c, where the spin-wave dispersion relation is reported, confirming the robustness of the spin-wave emission and propagation in magnetically nanopatterned spin textures for thick synthetic antiferromagnetic systems.

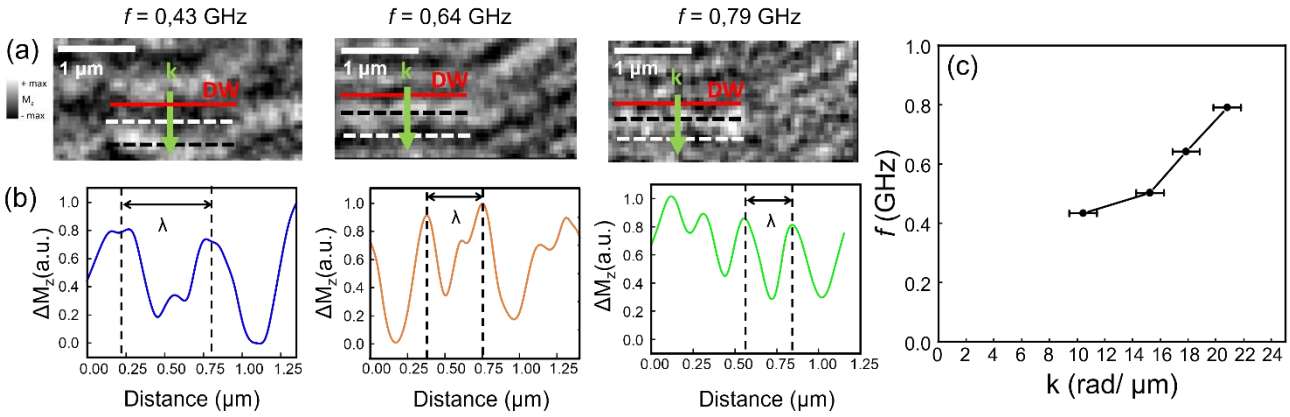

Figure 4: a. Scanning Transmission X-Ray Microscopy images of 2D planar propagating spin waves emitted from the domain wall in red at different excitation frequencies. The green arrow indicates the spin-wave wavevector k, while the white and black dashed lines show consecutive spin-wave wavefronts. b. Normalized spatial profiles of the spin waves extracted from (a) along the green arrow. c. Experimental spin-wave dispersion relation of the synthetic antiferromagnetic structure investigated.

5. CONCLUSION

In this work, we show that it is possible to control and engineer the emission and propagation of spin waves via the phase nanoengineering methodology, using tam-SPL in a 200 nm thick synthetic antiferromagnetic multilayer. In particular, we demonstrated that despite the smaller exchange bias interaction in comparison with thinner synthetic antiferromagnetic systems, it is still possible to pattern extremely stable magnetic domains, thanks to the flux closure state established inside the structure itself. Noteworthy, we show that different types of spin textures, such as vortices and domain walls, are extremely efficient and stable for the emission of coherent spin waves propagating for multiple wavelengths at different frequencies, with both radial and linear wavefronts. This opens up the possibility of using spin textures to excite and manipulate spin waves for the development of innovative nanodevices for spintronics. In addition to this, we demonstrate the robustness of spin-waves emission and propagation in synthetic antiferromagnetic systems with thickness up to few hundreds of nanometers. This allows to expand the comprehension of the spin-wave phenomenology to the third dimension, by studying the spin-wave dynamics with three-dimensional magnetic imaging techniques[31–35], mapping the complex spin-wave properties through the volume of the magnetic systems[22]. The ability to explore complex three-dimensional spin wave modes, and consequently to generate and manipulate new 3D spin-wave landscapes opens up unforeseen possibilities for the design of the next generation three-dimensional nanomagnonic computing architectures.

ACKNOWLEDGMENTS

This work was partially performed at PoliFAB, the microtechnology and nanotechnology centre of the Politecnico di Milano. The research leading to these results has received funding from the European Union's Horizon 2020 research and innovation programme under grant agreement number 948225 (project B3YOND). All synchrotron data was measured at the PolLux endstation of the Swiss Light Source, Paul Scherrer Institut, Villigen PSI, Switzerland. The PolLux endstation was financed by the German Bundesministerium für Bildung und Forschung (BMBF) through contracts 05K16WED and 05K19WE2. S.M. acknowledges funding from the Swiss National Science Foundation (Grant Agreement 172517).

COMPETING INTERESTS

Authors declare that they have no competing interests.

DATA AND MATERIALS AVAILABILITY

The data that support the findings of this study are available from corresponding authors DP and EA, upon reasonable request.

REFERENCES

[1] Prabhakar, A. & Stancil, D. D. Spin waves: Theory and applications. (Springer US, 2009). doi:10.1007/978-0-387-77865-5.

[2] Pirro, P., Vasyuchka, V.I., Serga, A.A. et al. Advances in coherent magnonics. Nat Rev Mater 6, 1114–1135 (2021). https://doi.org/10.1038/s41578-021-00332-w.

[3] Barman, A. et al. The 2021 Magnonics Roadmap. Journal of Physics: Condensed Matter 33, 413001 (2021).

[4] Wang, Q., Kewenig, M., Schneider, M. et al. A magnonic directional coupler for integrated magnonic half-adders. Nat Electron 3, 765–774 (2020). https://doi.org/10.1038/s41928-020-00485-6

[5] Lenk, B., Ulrichs, H., Garbs, F. & Münzenberg, M. The building blocks of magnonics. Physics Reports vol. 507, Issue 4-5 (2011).

[6] Klingler, S. et al. Spin-wave logic devices based on isotropic forward volume magnetostatic waves. Appl Phys Lett 106, (2015).

[7] Yu, H. et al. Omnidirectional spin-wave nanograting coupler. Nat Commun 4, (2013).

[8] Papp, Á., Porod, W. & Csaba, G. Nanoscale neural network using non-linear spin-wave interference. Nat Commun 12, 6422 (2021). https://doi.org/10.1038/s41467-021-26711-z.

[9] Vogt, K. et al. Spin waves turning a corner. Appl Phys Lett 101, (2012).

[10] Nakane, R., Tanaka, G. & Hirose, A. Reservoir Computing with Spin Waves Excited in a Garnet Film. IEEE Access 6, (2018).

[11] Petti, D. Building a half-adder based on spin waves. Nat Electron 3, 736–737 (2020). https://doi.org/10.1038/s41928-020-00514-4.

[12] Amelichev, V. V et al. Synthetic Antiferromagnetic Structures in Technology of Spintronic Devices. Nanobiotechnology Reports 16, 155–161 (2021).

[13] Duine, R.A., Lee, KJ., Parkin, S.S.P. et al. Synthetic antiferromagnetic spintronics. Nature Phys 14, 217–219 (2018). https://doi.org/10.1038/s41567-018-0050-y.

[14] Di, K. et al. Enhancement of spin-wave nonreciprocity in magnonic crystals via synthetic antiferromagnetic coupling. Sci Rep 5, (2015).

[15] Wintz, S., Tiberkevich, V., Weigand, M. et al. Magnetic vortex cores as tunable spin-wave emitters. Nature Nanotech 11, 948–953 (2016). https://doi.org/10.1038/nnano.2016.117

[16] Sluka, V., Schneider, T., Gallardo, R.A. et al. Emission and propagation of 1D and 2D spin waves with nanoscale wavelengths in anisotropic spin textures. Nat. Nanotechnol. 14, 328–333 (2019). https://doi.org/10.1038/s41565-019-0383-4

[17] Di, K. et al. Enhancement of spin-wave nonreciprocity in magnonic crystals via synthetic antiferromagnetic coupling OPEN. (2015) doi:10.1038/srep10153.

[18] Albisetti, E. et al. Optically Inspired Nanomagnonics with Nonreciprocal Spin Waves in Synthetic Antiferromagnets. Advanced Materials 32, 1906439 (2020).

[19] Petti, D., Tacchi, S. & Albisetti, E. Review on magnonics with engineered spin textures. J Phys D Appl Phys 55, 293003 (2022).

[20] Albisetti, E. et al. Nanopatterning spin-textures: A route to reconfigurable magnonics. AIP Adv 7, (2017).

[21] Albisetti, E., Petti, D., Pancaldi, M. et al. Nanopatterning reconfigurable magnetic landscapes via thermally assisted scanning probe lithography. Nature Nanotech 11, 545–551 (2016). https://doi.org/10.1038/nnano.2016.25
[22] Girardi, D. et al. Three-dimensional spin-wave dynamics, localization and interference in a synthetic antiferromagnet. arXiv:2306.15404 (2023).
[23] Levati, V. et al. Phase Nanoengineering via Thermal Scanning Probe Lithography and Direct Laser Writing. Adv Mater Technol 2300166 (2023) doi:10.1002/ADMT.202300166.
[24] Albisetti, E. et al. Thermal scanning probe lithography. Nature Reviews Methods Primers 2022 2:1 2, 1–21 (2022).
[25] Nogués, J. & Schuller, I. K. Exchange bias. J Magn Magn Mater 192, 203–232 (1999).
[26] Radu, F. & Zabel, H. Exchange bias effect of ferro-/antiferromagnetic heterostructures. Springer Tracts in Modern Physics 227, (2007).
[27] Albisetti, E. et al. Temperature Dependence of the Magnetic Properties of IrMn/CoFeB/Ru/CoFeB Exchange Biased Synthetic Antiferromagnets. Materials 13, (2020).
[28] Stiles, M. D. Interlayer exchange coupling. J Magn Magn Mater 200, 322–337 (1999).
[29] Gubbiotti, G. et al. Interlayer exchange coupling in Co/Ru/Co trilayers. J Magn Magn Mater 286, 468–472 (2005).
[30] Wang, Y., Levy, P. M. & Fry, J. L. Interlayer magnetic coupling in Fe/Cr multilayered structures. Phys Rev Lett 65, (1990).
[31] Manke, I. et al. Three-dimensional imaging of magnetic domains. Nat Commun 1, (2010).
[32] Donnelly, C. et al. Tomographic reconstruction of a three-dimensional magnetization vector field. New J Phys 20, (2018).
[33] Donnelly, C., Finizio, S., Gliga, S. et al. Time-resolved imaging of three-dimensional nanoscale magnetization dynamics. Nat. Nanotechnol. 15, 356–360 (2020). https://doi.org/10.1038/s41565-020-0649-x
[34] Popov, P. A. et al. Spin wave propagation in three-dimensional magnonic crystals and coupled structures. J Magn Magn Mater 476, 423–427 (2019).
[35] Donnelly, C., Guizar-Sicairos, M., Scagnoli, V. et al. Three-dimensional magnetization structures revealed with X-ray vector nanotomography. Nature 547, 328–331 (2017). https://doi.org/10.1038/nature23006